Optimal remediation design and simulation groundwater flow coupled to contaminant transport using genetic algorithm and radial point collocation method (RPCM)

Elsevier Editorial System(tm) for Science of the Total Environment
Manuscript Draft

Manuscript Number: STOTEN-D-18-07171

Title: Optimal remediation design and simulation groundwater flow coupled to contaminant transport using genetic algorithm and radial point collocation method (RPCM)

Article Type: VSI:Remediate MSCA

Keywords: Groundwater flow, Reactive contaminant transport, Radial basis function, Point collocation method, Genetic Algorithm

Corresponding Author: Professor Tim Ricken, Ph.D.

Corresponding Author's Institution: Stuttgart University

First Author: SeyedMorteza Seyedpour

Order of Authors: SeyedMorteza Seyedpour; P. Kirmizakis, MSC; P. Brennan, MSc.; R. Doherty, Phd.; Tim Ricken, Professor

Abstract: The simulation-optimization models of groundwater and contaminant transport can be
a powerful tool in the management of groundwater resources and remediation design.
In this study, using Multiquadratic Radial Basis Function (MRBF) a coupled groundwater flow and reactive transport of contaminant and oxidant was developed in the
framework of the Meshfree method. The parameter analysis has determined the optimum shape parameter (0.97), the results of the model were compared with a physical
sandbox model which were in good agreement. The Genetic Algorithm approach was
used to find the optimum design of the remediation using permanganate as an oxidant.
To find the optimum design we considered two objectives and two constraints. The
results revealed that the breakthrough of contaminant to the downstream area of interest and the concentration of the contaminant in this area is reduced significantly with
optimisation.

Suggested Reviewers: Ahmed Ashraf A. Phd.
assistant professor, Department of Civil engineering, Brunel University London, UK.
ashraf.ahmed@brunel.ac.uk
He is expert in Mathematical modeling of groundwater flow and mass transport in hydrogeologic systems by numerical methods including model development. Because of his publication in the field of numerical simulation of the contaminant transport.

Helmig Rainer Phd.
professor, Department of Hydromechanics and Modelling of Hydrosystems, University Stuttgart

Rainer.Helmig@iws.uni-stuttgart.de
He is head of department of Hydromechanics and Modelling of Hydrosystems at university of Stuttgart. His Department focuses on modelling of flow in porous media. Since one of our numerical approach is Theory of porous media, we recommend him as a reviewer.

Baskar Ganapathysubramanian Phd.
assistant professor, Department of Mechanical Engineering, 306 Lab of Mechanics, Iowa State Universit
baskarg@iastate.edu
He is expert in the computational mechanics and computational physics and their application in the contaminant transport.

F.W. Schwartz Phd.
professor, School of earth science, The Ohio State University
frank@geology.ohio-state.edu
Expert in the contaminant hydrology and different kind of remediation process especially ISCO.

G. R. Dodagoudar Phd.
assistant professor, Department of Civil Engineeri, Indian Institute of Technology Madras,Chennai,
goudar@iitm.ac.in
He is expert in CFD applications in environmental geotechnics and seismic hazard and risk assessment and has published many research papers in these fields.

Opposed Reviewers:

Cover Letter
Dear editor

I am enclosing herewith a manuscript entitled “Optimal remediation design and simulation of coupled groundwater flow and contaminant transport using genetic algorithm and radial point collocation method (RPCM)” submitted to “Science of the Total Environment” as an original article for possible evaluation.

In paper study, using Multiquadratic Radial Basis Function (MRBF) a coupled groundwater flow and reactive transport of contaminant and oxidant was developed in the framework of the Meshfree method. The parameter analysis has determined the optimum shape parameter (0.97), the results of the model were compared with a physical sandbox model which were in good agreement. The Genetic Algorithm approach was used to find the optimum design of the remediation using permanganate as an oxidant. To find the optimum design we considered two objectives and two constraints. The results revealed that the breakthrough of contaminant to the downstream area of interest and the concentration of the contaminant in this area is reduced significantly with optimisation.

With the submission of this manuscript, I would like to undertake that the above the mentioned manuscript has not been published elsewhere, accepted for publication

elsewhere or under editorial review for publication elsewhere; and that all contributors

are fully aware of this submission.

All authors were fully involved in the study and preparation of the manuscript, and there is no conflict of interest.

Thank you for time and consideration
Tim Ricken
Head of Institute of Statics and Dynamics of Aerospace Structures
Faculty of Aerospace Engineering and Geodesy, University of Stuttgart, Pfaffenwaldring 27, 70569 Stuttgart,Germany.
Tel: +49-(0)711685-63612
E-mail: ricken@isd.uni-stuttgart.de

*Title Page

Optimal remediation design and simulation groundwater flow coupled to contaminant transport using genetic algorithm and radial point collocation method (RPCM)

***Graphical Abstract**

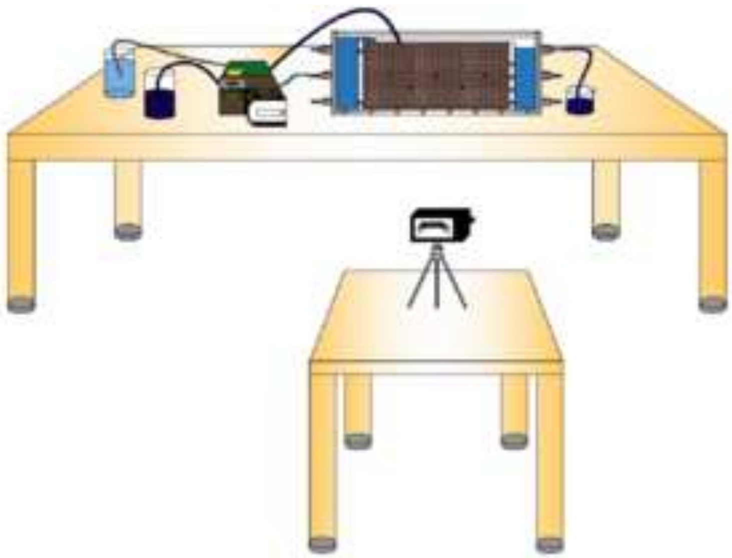

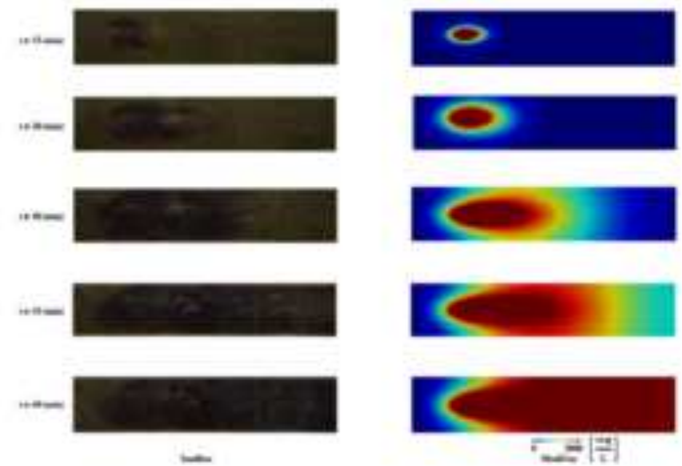

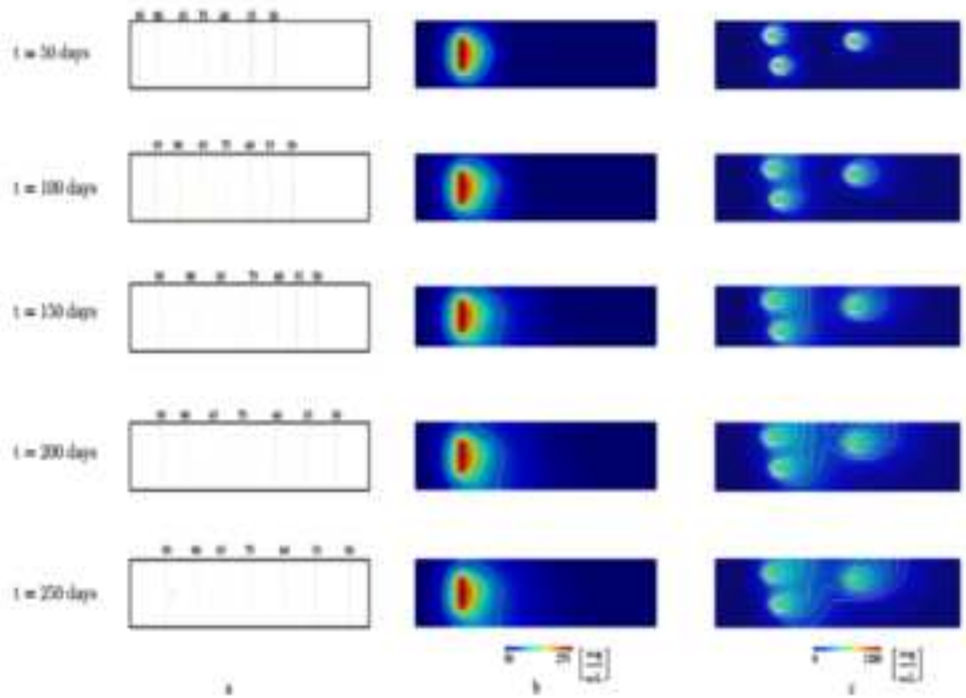

***Highlights (for review : 3 to 5 bullet points (maximum 85 characters including spaces per bullet point)**

- Using Multiquadratic Radial Basis Function (MRBF) a coupled groundwater flow and reactive transport of contaminant and oxidant was developed in the framework of the Meshfree method.
- The parameter analysis has determined the optimum shape parameter (0.97), the results of the model were compared with a physical sandbox model which were in good agreement.
- The Genetic Algorithm approach was used to find the optimum design of the remediation using permanganate as an oxidant.
- To find the optimum design we considered two objectives and two constraints.

Optimal remediation design and simulation groundwater flow coupled to contaminant transport using genetic algorithm and radial point collocation method (RPCM)

S.M. Seyedpour[a], P. Kirmizakis[b], P. Brennan[c], R. Doherty[b], T. Ricken[d,*]

[a]Institute of Mechanics, Structural Analysis, and Dynamics, TU Dortmund University, 44227 Dortmund, Germany
[b]School of Natural and Built Environment, Queen's University Belfast, BT9 5AG, United Kingdom
[c]School of Chemical Sciences, Dublin City University, Glasnevin, Dublin 9, Ireland
[d]Institute of Mechanics, Structural Analysis and Dynamics, Faculty of Aerospace Engineering and Geodesy, University of Stuttgart, 70569 Stuttgart, Germany

Abstract

The simulation-optimization models of groundwater and contaminant transport can be a powerful tool in the management of groundwater resources and remediation design. In this study, using Multiquadratic Radial Basis Function (MRBF) a coupled groundwater flow and reactive transport of contaminant and oxidant was developed in the framework of the Meshfree method. The parameter analysis has determined the optimum shape parameter (0.97), the results of the model were compared with a physical sandbox model which were in good agreement. The Genetic Algorithm approach was used to find the optimum design of the remediation using permanganate as an oxidant. To find the optimum design we considered two objectives and two constraints. The results revealed that the breakthrough of contaminant to the downstream area of interest and the concentration of the contaminant in this area is reduced significantly with optimisation.

Keywords: Groundwater flow, Reactive contaminant transport, Radial basis function, Point collocation method, Genetic Algorithm

*Corresponding author
Email addresses: seyedmorteza.seyedpour@tu-dortmund.de (S.M. Seyedpour), pkirmizakis01@qub.ac.uk (P. Kirmizakis), peter.brennan234@mail.dcu.ie (P. Brennan), r.doherty@qub.ac.uk (R. Doherty), ricken@isd.uni-stuttgart.de (T. Ricken)

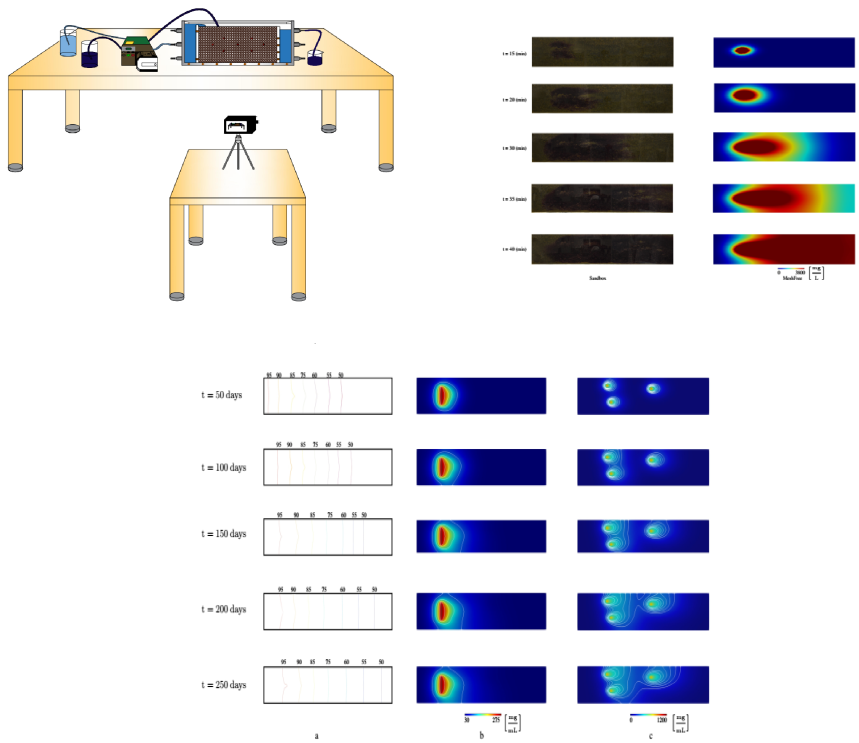

Figure 1: Graphical abstract

1. Introduction

Groundwater is a primary resource for drinking water, agriculture and industry (An et al., 2013; Zhang et al., 2017), and its contamination can have long-term negative influences on the environment causing severe disasters (Chen et al., 2017; Elimelech and Phillip, 2011). Aside from pollution issues, the water scarcity in freshwater lakes, rivers and aquifers, namely blue water, due to droughts (**?**) and greater demand because of intensive industrial and economic growth (**?**), namely water stress, have increased the importance of proactively protecting uncontaminated groundwater sources and reactively remediating contaminated sources. Thus, the selection of a remediation technology among different remedial strategies and optimising remediation design, are challenging issues with which decision-makers currently struggle (Hadley and Newell, 2012; Stroo et al., 2012). Numerical modeling of groundwater flow and contaminant transport can play a crucial role in groundwater management (Wang and Anderson, 1982). The results of simulations can not only reveal the behaviour of contaminant migration through the porous media with respect to space and time but also can be used to optimise the remediation process. Furthermore, coupled simulation-optimization approaches for groundwater flow, contaminant fate and remediation technologies can address uncertainties in remediation design and reduce expenses (Tam and Byer, 2002; Ba and Mayer, 2007; He et al., 2009). The groundwater flow and contaminant transport, mathematically, can be expressed by differential equations considering dispersion, advection, sorption, reaction, degradation, etc (Sun and Sun, 2013; Sharma and Reddy, 2004). In general, there are two different approaches to solve these equations, analytical and numerical methods. The analytical approaches are applicable only when the boundary conditions and the geometries are simplified (Zheng and Bennett, 2002), while the numerical strategies can be applied to many sophisticated problems. There are different numerical approaches, including finite difference method (FDM) (Tatalovich et al., 2000), finite volume method (FVM) (Bertolazzi and Manzini, 2004), finite element method (FEM) (Robeck et al., 2011; Ricken et al., 2014; SCHMUCK et al., 2016; Seyedpour and Ricken, 2016), and boundary element method (BEM) (Leo and Booker, 1998) which can be used to solve the governing equation of groundwater flow and contaminant transport. Although their success in dealing with geometry complexity and heterogeneity they encounter some difficulties in a simulation of high advection velocities and the low diffusion resulting in high Peclet number and also low dispersivities.

Recently, Meshfree methods, in addition to other numerical techniques, have become popular in groundwater modelling. In contrast to the grid or mesh-based approaches, Meshfree methods, do not suffer from shortcomings such as numerical dispersion, meshing, remeshing in FDM and FEM which often lead to substantial cost and time in the adaptive analysis, and limitation in some problems such as large deformation and the breakage of material (Liu and Gu, 2005). Meshless techniques include the smooth-particle hydrodynamics, kernel method, moving least squares method, the element-free Galerkin method, partition of unity method, local Petrov-Galerkin method and point collocation method. Each method has its own merits and disadvantages in particular problems. The solution procedure in the Meshfree methods departs from FEM in the geometry representation and shape function construction. In the Meshfree methods, instead of meshes, the geometry and its boundary are represented by nodes. Polynomial basis functions and radial basis functions (RBF) have often been used to construct shape functions to approximate the unknown field parameters in the point collocation method. These functions have also been utilized for groundwater modelling in many studies. Kumar et al. investigated a Meshfree simulation for contaminant transport through saturated porous media using thin plate spline radial basis functions to construct shape functions. The authors validated their simulation with experimental results. Their results were in good agreement with FEM simulation (Praveen Kumar and Dodagoudar, 2008). Meenal and Eldho developed a meshfree model using multiquadric radial basis functions based on collocation method to simulate groundwater flow in an unconfined aquifer (Meenal and Eldho, 2011). They have extended their model for the two-dimensional coupled groundwater flow and transport simulation in an unconfined aquifer and verified the accuracy of their model with analytical solutions (Meenal and Eldho, 2012). Singh et al. developed the RPCM method for coupled groundwater flow and contaminant transport simulation in a confined aquifer in steady state and compared their results with experimental results (Guneshwor Singh et al., 2016). Yao et al. presented RBF mesh free description for reactive transport of dioxin as a contaminant and slow release of permanganate as an oxidant to better understand the design for large scale contaminated sites (Yao et al., 2016).

Traditional mathematical methods, used to optimize the problems in different areas of engineering practices, have lost their effectiveness as problems have become more complex; hence other optimization algorithms such as natural computing are investigated. Natural computing methods are one class of biomimicry optimisation methods such as genetic algorithm (GA), particle swarm optimisation (PSO), differential evolution and artificial bee colony are effective methods to optimise complicated environmental problems such as groundwater remediation process. Genetic Algorithms, introduced by Holland (Holland, 1992), is one of the functional natural computing methods belongs to the evolutionary computing algorithms. Genetic Algorithms, which is based on the theory of evolution, mimic natural evolution or information handling with respect to problems in other scientific areas such as environmental engineering (Sotomayor et al., 2018; Varghese et al., 2015). By utilizing genetic principles including selection, population, crossover and mutation, this method finds optimum solutions to problems, and in our study, this solution discovers the optimal number and design for oxidant resources. The genetic algorithm begins the solution process by selecting a relatively small population in which every individual represents a possible solution in the parameter space, and the efficiency of each individual is determined using objective functions. The new generation is reproduced by utilising probability rules in the combination of the concept of selection, crossover and mutation leading to decrease the survival chance of the less fit individuals.

Sinha et al. developed a multiscale island injection genetic algorithm (IIGA) and tested it using a field-scale pump-and-treat design problem at the Umatilla Army Depot in Oregon, USA (Sinha and Minsker, 2007). He et al. investigated their one previous works (Huang, 1992; He et al., 2008b,a) to optimise the design of field-scale pump and treat system (PAT). The authors simulated the transport of petroleum as a contaminant and assumed the porosity of the soil to be stochastic variables with normal distribution (He et al., 2009). They found that the remediation cost might increase because of the effects of uncertainty. With the aid of the knowledge of forensic observations, Tian et al. used quantum-behaved particle swarm optimization to solve an inverse advection-dispersion problem of estimating the strength of time-varying groundwater contaminant source. They concluded that the proposed method can be used efficiently to reconstruct the contaminant source history. (Tian et al., 2011).

It is natural for decision makers to want assurance that the numerical models are valid. To validate the numerical approaches, analytical solution, real field data and a physical model such as sandbox experiment can be used. The Sandbox experiment can be used not only as an experimental method for validating simulations but also visualising, predicting (Illman et al., 2012) a solute transport.

The outline of this paper is as follows. The governing equations of the coupled groundwater flow and reactive transport are introduced in section 2. In section 3 the RPCM discretization of these equations is described. The sandbox experiment which is used to validate the results is presented in section 4. The genetic algorithm approach used to find the optimum location of the oxidant sources is illustrated in section 5. Finally, the results and discussions are presented in section 6 , and conclusions are given in section 7.

2. Governing equations and boundary conditions

2.1. Groundwater flow

The transient flow of groundwater through a saturated, anisotropic, inhomogeneous, porous aquifer in 2D can be written as (Bear, 1979, 2007)

$$\frac{\partial}{\partial \mathrm{x}}\left[\mathrm{k_x}\frac{\partial \mathrm{h}}{\partial \mathrm{x}}\right]+\frac{\partial}{\partial \mathrm{y}}\left[\mathrm{k_y}\frac{\partial \mathrm{h}}{\partial \mathrm{y}}\right]=\mathrm{S}\frac{\partial \mathrm{h}}{\partial \mathrm{t}}+\mathrm{Q_w}\left(\mathrm{x}-\mathrm{x_i}\right)\left(\mathrm{y}-\mathrm{y_i}\right)-\mathrm{q}. \tag{1}$$

where $\mathrm{h}(\mathrm{x},\mathrm{y},\mathrm{t})$ is the piezometric head $[\mathrm{L}]$, $\mathrm{k_x}$ and $\mathrm{k_y}$ are hydraulic conductivity in x and y direction $\left[\mathrm{LT^{-1}}\right]$, S is the storage coefficient, $\mathrm{Q_w}$ is the source or sink term $\left[\mathrm{L^3T^{-1}L^{-2}}\right]$ and q denotes the recharge rate $\left[\mathrm{LT^{-1}}\right]$.

Where Ω and $\partial\Omega$ are the aquifer domain and its Lipschitz continuous boundary respectively. $\partial\Omega$ comprises of $\partial\Omega=\Gamma_\mathrm{D}\oplus\Gamma_\mathrm{N}$, where Γ_D and Γ_N interpret the portions of Γ in which Dirichlet and Neumann boundary conditions on groundwater flow and contaminant transport equations are imposed (Fig. 2) :

$$\mathrm{h}(\mathrm{x},\mathrm{y},0)=\mathrm{h_0}(\mathrm{x},\mathrm{y}), \qquad (\mathrm{x},\mathrm{y})\in\Omega. \tag{2}$$

$$\mathrm{h}(\mathrm{x},\mathrm{y},\mathrm{t})=\mathrm{h_1}(\mathrm{x},\mathrm{y}), \qquad (\mathrm{x},\mathrm{y})\in\Gamma_\mathrm{D}. \tag{3}$$

$$\mathrm{k_y}\frac{\partial \mathrm{h}}{\partial \mathrm{y}}=0, \qquad (\mathrm{x},\mathrm{y})\in\Gamma_N. \tag{4}$$

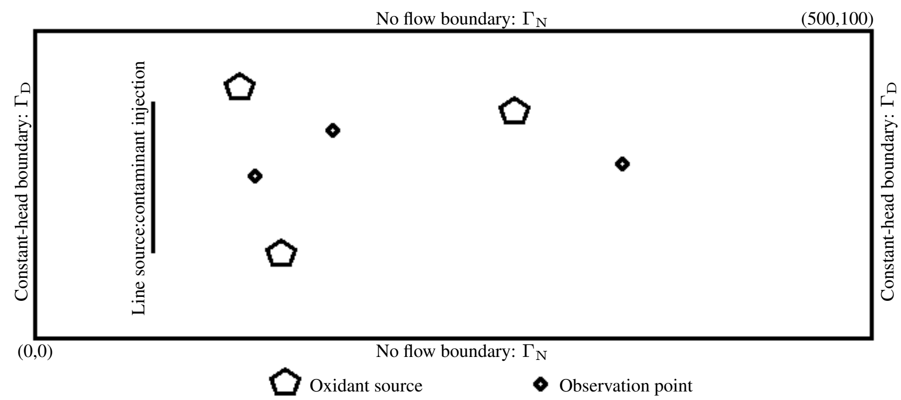

Figure 2: The aquifer domain and physical setting of the model

2.2. Reactive transport

Reactive transport of the contaminant and oxidant in groundwater is given by the following coupled advection−dispersion equations (Freeze and Cherry, 1979; Wang and Anderson, 1982) :

$$
\begin{aligned}
\mathrm{R}\frac{\mathrm{n^F}}{\mathrm{n^S}}\frac{\partial \mathrm{C}^1}{\partial \mathrm{t}} = \frac{\partial}{\partial \mathrm{x}}\left[\mathrm{D_{xx}}\frac{\partial \mathrm{C}^1}{\partial \mathrm{x}}\right] + \frac{\partial}{\partial \mathrm{y}}\left[\mathrm{D_{yy}}\frac{\partial \mathrm{C}^1}{\partial \mathrm{y}}\right] - \frac{\partial}{\partial \mathrm{x}}\left[v_x \mathrm{C}^1\right] \\
- \frac{\partial}{\partial \mathrm{y}}\left[v_y \mathrm{C}^1\right] - \mathrm{K}\mathrm{C}^1\mathrm{C}^2.
\end{aligned}
\tag{5}
$$

$$
\begin{aligned}
\mathrm{R}\frac{\mathrm{n^F}}{\mathrm{n^S}}\frac{\partial \mathrm{C}^2}{\partial \mathrm{t}} = \frac{\partial}{\partial \mathrm{x}}\left[\mathrm{D_{xx}}\frac{\partial \mathrm{C}^2}{\partial \mathrm{x}}\right] + \frac{\partial}{\partial \mathrm{y}}\left[\mathrm{D_{yy}}\frac{\partial \mathrm{C}^2}{\partial \mathrm{y}}\right] - \frac{\partial}{\partial \mathrm{x}}\left[v_x \mathrm{C}^2\right] \\
- \frac{\partial}{\partial \mathrm{y}}\left[v_y \mathrm{C}^2\right] - \mathrm{K}\mathrm{C}^1\mathrm{C}^2 + \mathrm{F_{release}}\delta\left(\mathrm{x} - \mathrm{x_i}\right)\left(\mathrm{y} - \mathrm{y_i}\right).
\end{aligned}
\tag{6}
$$

where R is retardation factor and describes sorption, $\mathrm{n^F}$ and $\mathrm{n^S}$ are volume fractions of groundwater and soil respectively, and their fraction $\dfrac{\mathrm{n^F}}{\mathrm{n^S}}$ denotes the porosity of the aquifer, $\mathrm{D_x}$ and $\mathrm{D_y}$ are components of dispersion coefficient tensor in x and y directions respectively. $\left[\mathrm{L^2T^{-1}}\right]$, C^1 and C^2 are concentration of 1,4-Dioxacyclohexane $(\mathrm{C_4H_8O_2})$ as a contaminant and permanganate as an oxidant respectively $\left[\mathrm{ML^{-3}}\right]$, k is second order reaction constant $\left[\mathrm{T^{-1}}\right]$ and $\mathrm{F_{Release}}$ is the release function of permanganate (Wolf, 2013). v_x and v_y are seepage velocity vectors in x and y directions respectively $\left[\mathrm{LT^{-1}}\right]$ evaluated from the solutions of the flow equations using the following relations (Bear, 1979, 2007):

$$
\mathrm{v_x} = -\mathrm{k_x}\,\frac{\partial \mathrm{h}}{\partial \mathrm{x}} \quad ; \quad \mathrm{v_y} = -\mathrm{k_y}\,\frac{\partial \mathrm{h}}{\partial \mathrm{y}}. \tag{7}
$$

where $\mathrm{k_x}$ and $\mathrm{k_y}$ are the hydraulic conductivities in x and y directions respectively.The components of the dispersion coefficient tensor , $\mathbf{D} = \mathbf{D}\,(\mathsf{x})$, are evaluated using the following relations:

$$\mathrm{D_{xx}} = \frac{\alpha_\mathrm{L}\mathrm{v_x}^2 + \alpha_\mathrm{T}\mathrm{v_y}^2}{\sqrt{\mathrm{v_x}^2 + \mathrm{v_y}^2}} + \mathrm{D}^* \ ; \ \mathrm{D_{yy}} = \frac{\alpha_\mathrm{L}\mathrm{v_y}^2 + \alpha_\mathrm{T}\mathrm{v_x}^2}{\sqrt{\mathrm{v_x}^2 + \mathrm{v_y}^2}} + \mathrm{D}^*. \tag{8}$$

where α_L and α_T are longitudinal and transverse dispersivity and D^* is the effective molecular diffusion coefficient. v_x and v_y in Eqs.(7) and (8) are evaluated from the flow equation and these two equations couple the groundwater flow and reactive transport.

For transient analysis of reactive transport, the following initial and boundary conditions are specified:

$$\mathrm{C}^1(\mathrm{x},\mathrm{y},0) = 0 \quad ; \quad \mathrm{C}^2(\mathrm{x},\mathrm{y},0) = 0, \quad (\mathrm{x},\mathrm{y}) \in \Omega. \tag{9}$$

$$\mathrm{C}^1(4,\mathrm{y},\mathrm{t})\,|_{1<\mathrm{y}<3} = \hat{\mathrm{C}}^1. \tag{10}$$

$$\mathrm{C}^2(\mathrm{x},\mathrm{y},\mathrm{t}) = \begin{cases} \mathrm{f(t)_{release}} & (\mathrm{x},\mathrm{y})\ \text{in Oxidan source} \\ 0 & \end{cases} \tag{11}$$

$$\frac{\partial \mathrm{C}^1}{\partial \mathrm{y}} = 0 \ ; \ \frac{\partial \mathrm{C}^2}{\partial \mathrm{y}} = 0, \qquad (\mathrm{x},\mathrm{y}) \in \Gamma_N. \tag{12}$$

3. RPCM formulation

3.1. Radial basis function interpolation

In the Meshfree method, the problem domain and its boundaries are represented by a set of nodes, namely field nodes, scattered within the problem domain and its boundaries. The initial step to solve PDEs through the Meshfree method is the approximation of unknown field variables using trial or shape function. To approximate the function values at node x, a set of neighbourhood nodes called local support domains are used to construct shape functions but the shape functions outside of the local support domains are regarded as zero. In contrast to the finite element method in which the shape function is the same for the entire elements, in the Meshfree method, the shape functions and the local support domains can change for a different point of interest. Fig. 2. illustrates various types of local support domains used in the Meshfree method.

Among these support domains, circular and rectangular support domains are more common. To construct Meshfree shape functions used in the point interpolation method, two different types of basis functions, namely Radial basis function (JG Wang, 2002) and polynomial basis, (GR, 1999) have been investigated. To approximate the piezometric head, the following linear combination of the radial and polynomial basis functions can be used (Liu and Gu, 2005):

$$\mathrm{h}(\mathbf{x}) = \sum_{\mathrm{i}=1}^{\mathrm{n}} \mathrm{a_i R_i}(\mathbf{x}) + \sum_{\mathrm{j}=1}^{\mathrm{n}} \mathrm{P_i}(\mathbf{x}\mathrm{b_i}) = \mathbf{R}^\mathrm{T}(\mathbf{x})\,\mathbf{a} + \mathbf{P}^\mathrm{T}(\mathbf{x})\,\mathbf{b}. \tag{13}$$

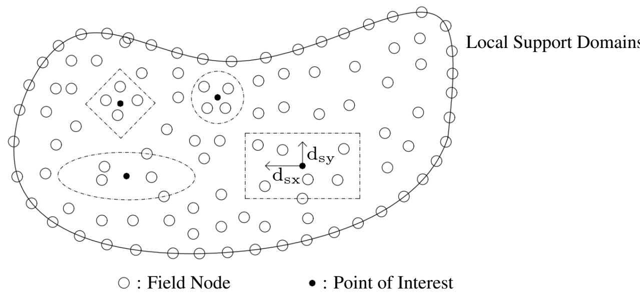

Figure 3: Different local support domains used in Meshfree methods.

where $\mathrm{R}(\mathbf{x})$ and $\mathrm{P}(\mathbf{x})$ denote radial basis and polynomial basis functions respectively, n is the number of RBFs, m is the number of polynomials where m is usually smaller than n and when $\mathrm{m} = 0$, the interpolation is dominated only by pure RBFs. Coefficients $\mathrm{a_i}$ and $\mathrm{b_i}$ are constants which can be determined by enforcing the interpolation function passing through all nodes within the support domain.

There are four common types of RBFs whose characteristics have been investigated in many studies (Kansa, 1990; Schaback and Wendland, 2000; Hardy, 1971) including the multi-quadrics (MQ) function, the exponential or Gaussian (Exp) function, the thin plate spline (TPS) function, and the Logarithmic radial basis function. In all RBFs, the only variable is the distance between the point of interest $\mathbf{x}$ and a node located at $\mathbf{x_i}$ that can be expressed as:

$$\mathrm{r} = \sqrt{\left(\mathrm{x} - \mathrm{x_i}\right)^2 + \left(\mathrm{y} - \mathrm{y_i}\right)^2}, \qquad \text{for 2D Problems.} \tag{14}$$

In our study, among different radial basis functions, we have chosen multi-quadrics which is defined as below:

$$\mathrm{R_i}\left(\mathrm{x}, \mathrm{y}\right) = \left(\mathrm{r_i}^2 + \left(\alpha_\mathrm{c}\mathrm{d_c}\right)^2\right)^\mathrm{q}. \tag{15}$$

where α_c, $\mathrm{d_c}$ and q are the shape parameters. α_c controls the size of support domain, and $\mathrm{d_c}$ is the average nodal spacing in the support domain near the point of interest, and it is defined using the following equation:

$$\mathrm{d_c} = \frac{\sqrt{\mathrm{A_s}}}{\sqrt{\mathrm{n_{A_s}}} - 1}. \tag{16}$$

where $\mathrm{A_s}$ is the area of the estimated support domain and $\mathrm{n_{A_s}}$ is the number of nodes embraced by the estimated area of $\mathrm{A_s}$. Among different support domains used to construct shape functions, we have chosen the rectangular domain which is easy to build and implement. The dimension of the rectangular support domain is determined by the following relations:

$$\begin{aligned} \mathrm{d_{sx}} &= \alpha_\mathrm{Cx}\mathrm{d_{cx}}. \\ \mathrm{d_{sy}} &= \alpha_\mathrm{Cy}\mathrm{d_{cy}}. \end{aligned} \tag{17}$$

where $\mathrm{d_{cx}}$ and $\mathrm{d_{cy}}$ are nodal spacing in x and y directions (Fig.2). Shape parameters play a crucial role in the accuracy of numerical solutions while RBFs are used in Meshfree methods. Although there is no established method to choose the optimum value for shape parameter, some studies have been conducted to find the optimum shape parameter for specific types of problems (Rippa, 1999; Wang and Liu, 2002; Wright, 2003). The unknown coefficients $\mathrm{a_i}$ and $\mathrm{b_j}$ in Eq.(13) are established by enforcing the interpolation function passing through all n scattered nodes within the support domain leading to n algebraic equations expressed in matrix form as:

$$\mathbf{h}^{\mathrm{T}} = \mathbf{R_Q a} + \mathbf{P_m b}. \tag{18}$$

The moment matrices corresponding to the radial basis function $\mathbf{R_Q}$ and the polynomial basis function $\mathbf{P_Q}$ are expressed by the following relations:

$$\begin{aligned}
\mathbf{R_Q} &= \begin{bmatrix} \mathrm{R_1(x_1, y_1)} & \mathrm{R_2(x_1, y_1)} & . & \mathrm{R_n(x_1, y_1)} \\ \mathrm{R_1(x_2, y_2)} & \mathrm{R_2(x_2, y_2)} & . & \mathrm{R_n(x_2, y_2)} \\ . & . & . & . \\ \mathrm{R_1(x_n, y_n)} & \mathrm{R_2(x_n, y_n)} & . & \mathrm{R_n(x_n, y_n)} \end{bmatrix}_{n\times n}, \\
\mathbf{P_m} &= \begin{bmatrix} \mathrm{P_1(x_1, y_1)} & \mathrm{P_2(x_1, y_1)} & . & \mathrm{P_m(x_1, y_1)} \\ \mathrm{P_1(x_2, y_2)} & \mathrm{P_2(x_2, y_2)} & . & \mathrm{P_m(x_2, y_2)} \\ . & . & . & . \\ \mathrm{P_1(x_n, y_n)} & \mathrm{P_2(x_n, y_n)} & . & \mathrm{P_m(x_n, y_n)} \end{bmatrix}_{n\times m}.
\end{aligned} \tag{19}$$

There is $\mathrm{n + m}$ unknowns in Eq.(18) and in order to determine all the unknowns, the following m additional equations need to be added to the system equations:

$$\sum_{i=1}^{n} \mathrm{p_j}(\mathbf{x_i})\, \mathrm{a_i} = \mathrm{P_m^T}\mathbf{a} = 0, \quad \mathrm{j = 1, 2, ..., m}. \tag{20}$$

Eq.(17) and Eq.(20) together can be written as below:

$$\begin{bmatrix} \mathbf{R_Q} & \mathbf{P_m} \\ \mathbf{P_m^T} & \mathbf{0} \end{bmatrix} \begin{Bmatrix} \mathbf{a} \\ \mathbf{b} \end{Bmatrix} = \begin{Bmatrix} \mathbf{h^T} \\ 0 \end{Bmatrix}. \tag{21}$$

substituting unknown coefficients into Eq.(13), the interpolation can be written as:

$$\mathbf{h}(\mathbf{x}) = \mathbf{\Xi^T}(\mathbf{x})\mathbf{h_s}. \tag{22}$$

where $\mathbf{\Xi}(\mathbf{x})$, are the shape functions and expressed as:

$$\mathbf{\Xi}(\mathbf{x}) = \{\mathit{\Xi}_1(\mathrm{x, y})\, \mathit{\Xi}_2(\mathrm{x, y}) \ldots \mathit{\Xi}_n(\mathrm{x, y})\}. \tag{23}$$

and, $\mathbf{h_s} = \{\mathrm{h_1 h_2 ... h_n}\}$ is the nodal head values vector at the support domain nodes. The first and second derivatives of piezometric head in x and y directions at any point can be expressed by the following equations:

$$\begin{aligned}
\frac{\partial \mathbf{h_l}}{\partial \mathrm{x}} &= \frac{\partial \mathbf{\Xi^T}}{\partial \mathrm{x}} \mathbf{h_s} = \sum_{i=1}^{n} \frac{\partial \Xi_i}{\partial \mathrm{x}} \mathrm{h_i} \quad ; \quad \frac{\partial^2 \mathbf{h_l}}{\partial \mathrm{x}^2} = \frac{\partial^2 \mathbf{\Xi^T}}{\partial \mathrm{x}^2} \mathbf{h_s} = \sum_{\mathrm{i=1}}^{\mathrm{n}} \frac{\partial^2 \Xi_{\mathrm{i}}}{\partial \mathrm{x}^2} \mathrm{h_i}. \\
\frac{\partial \mathbf{h_l}}{\partial \mathrm{y}} &= \frac{\partial \mathbf{\Xi^T}}{\partial \mathrm{y}} \mathbf{h_s} = \sum_{i=1}^{n} \frac{\partial \Xi_i}{\partial \mathrm{y}} \mathrm{h_i} \quad ; \quad \frac{\partial^2 \mathbf{h_l}}{\partial \mathrm{y}^2} = \frac{\partial^2 \mathbf{\Xi^T}}{\partial \mathrm{y}^2} \mathbf{h_s} = \sum_{\mathrm{i=1}}^{\mathrm{n}} \frac{\partial^2 \Xi_{\mathrm{i}}}{\partial \mathrm{y}^2} \mathrm{h_i}.
\end{aligned} \tag{24}$$

3.2. Discretisation of governing equations

3.2.1. Time discretisation

The time discretisation has been executed using the widely known Crank-Nicholson time stepping method in which the time derivative is replaced with a simple forward difference while the solution is replaced with a weighted value of the previous time-step solution, and the current solution expressed by the following equations:

$$
\begin{aligned}
&\frac{\mathrm{h}}{\partial \mathrm{t}}=\frac{\mathrm{h}^{t+\Delta \mathrm{t}}-\mathrm{h}^{t}}{\Delta \mathrm{t}}, \\
&\mathrm{h}=\frac{\mathrm{h}^{t+\Delta \mathrm{t}}-\mathrm{h}^{t}}{2}.
\end{aligned}
\tag{25}
$$

3.2.2. RPCM approximation

By the collocation of groundwater flow equation at all internal nodes using Eq.(22), the following discretised form of the piezometric head can be written:

$$
\mathrm{k}\left(\mathbf{x}_{\mathrm{r}}\right)\left[\frac{\partial^{2} \boldsymbol{\Xi}^{\mathrm{T}}}{\partial \mathrm{x}^{2}}+\frac{\partial^{2} \boldsymbol{\Xi}^{\mathrm{T}}}{\partial \mathrm{y}^{2}}\right] \mathbf{h}_{\mathrm{s}}(\mathrm{t})=\mathrm{S}\left(\mathbf{x}_{\mathrm{r}}\right)\left(\frac{\partial \mathrm{h}}{\partial \mathrm{t}}\right)+\mathrm{Q}_{\mathrm{w}} \delta\left(\mathbf{x}_{\mathrm{r}}-\mathbf{x}_{\mathrm{i}}\right)-\mathrm{q}\left(\mathbf{x}_{\mathrm{r}}\right). \tag{26}
$$

Substituting Eq.(25), the following equation is achieved:

$$
\begin{aligned}
&\frac{1}{2} \mathrm{k}\left(\mathbf{x}_{\mathrm{r}}\right)\left[\frac{\partial^{2} \boldsymbol{\Xi}^{\mathrm{T}}}{\partial \mathrm{x}^{2}}+\frac{\partial^{2} \boldsymbol{\Xi}^{\mathrm{T}}}{\partial \mathrm{y}^{2}}\right] \mathbf{h}_{\mathrm{s}}^{\mathrm{t}+\Delta \mathrm{t}}+\frac{1}{2} \mathrm{k}\left(\mathbf{x}_{\mathrm{r}}\right)\left[\frac{\partial^{2} \boldsymbol{\Xi}^{\mathrm{T}}}{\partial \mathrm{x}^{2}}+\frac{\partial^{2} \boldsymbol{\Xi}^{\mathrm{T}}}{\partial \mathrm{y}^{2}}\right] \mathbf{h}_{\mathrm{s}}^{\mathrm{t}} \\
&=\mathrm{S}_{\mathrm{r}}\left(\frac{\boldsymbol{\Xi}^{\mathrm{T}} \mathbf{h}_{\mathrm{s}}^{\mathrm{t}+\Delta \mathrm{t}}-\mathrm{h}_{\mathrm{r}}^{\mathrm{t}}}{\Delta \mathrm{t}}\right)+\mathrm{Q}_{\mathrm{w}} \delta\left(\mathbf{x}_{\mathrm{r}}-\mathbf{x}_{\mathbf{i}}\right)-\mathrm{q}_{\mathrm{r}}.
\end{aligned}
\tag{27}
$$

A similar approach is performed to discretise reactive transport equations, and the equations below are achieved:

$$
\mathrm{C}^{\mathrm{j}}(\mathrm{x}, \mathrm{t})=\sum_{\mathrm{i}=1}^{\mathrm{n}} \Xi_{\mathrm{i}}(\mathbf{x}) \mathrm{C}_{\mathrm{i}}^{\mathrm{j}}(\mathrm{t})=\boldsymbol{\Xi}^{\mathrm{T}} \mathbf{C}_{\mathrm{s}}^{\mathrm{j}}, \qquad \mathrm{j}=1,2. \tag{28}
$$

$$
\begin{aligned}
&\mathrm{R} \frac{\mathrm{n}^{\mathrm{f}}}{\mathrm{n}^{\mathrm{s}}} \frac{\boldsymbol{\Xi}^{\mathrm{T}} \mathbf{C}_{\mathbf{s}}^{\mathbf{1}}-\mathrm{C}_{\mathrm{r}}^{1 \mathrm{t}}}{\Delta \mathrm{t}}=\frac{1}{2}\left[\mathrm{D}_{\mathrm{xx}_{\mathrm{r}}} \frac{\partial^{2} \boldsymbol{\Xi}^{\mathrm{T}}}{\partial \mathrm{x}^{2}}+\mathrm{D}_{\mathrm{yy}_{\mathrm{r}}} \frac{\partial^{2} \boldsymbol{\Xi}^{\mathrm{T}}}{\partial \mathrm{y}^{2}}\right] \mathbf{C}_{\mathrm{s}}^{1\ \mathrm{t}+\Delta \mathrm{t}}+ \\
&\frac{1}{2}\left[\mathrm{D}_{\mathrm{xx}_{\mathrm{r}}} \frac{\partial^{2} \boldsymbol{\Xi}^{\mathrm{T}}}{\partial \mathrm{x}^{2}}+\mathrm{D}_{\mathrm{yy}_{\mathrm{r}}} \frac{\partial^{2} \boldsymbol{\Xi}^{\mathrm{T}}}{\partial \mathrm{y}^{2}}\right] \mathbf{C}_{\mathrm{s}}^{1\ \mathrm{t}}-\frac{1}{2}\left[\mathrm{v}_{\mathrm{x}_{\mathrm{r}}} \frac{\partial \boldsymbol{\Xi}^{\mathrm{T}}}{\partial \mathrm{x}}+\mathrm{v}_{\mathrm{y}_{\mathrm{r}}} \frac{\partial \boldsymbol{\Xi}^{\mathrm{T}}}{\partial \mathrm{y}}\right] \mathbf{C}_{\mathrm{s}}^{1\ \mathrm{t}+\Delta \mathrm{t}}- \\
&\frac{1}{2}\left[\mathrm{v}_{\mathrm{x}_{\mathrm{r}}} \frac{\partial \boldsymbol{\Xi}^{\mathrm{T}}}{\partial \mathrm{x}}+\mathrm{v}_{\mathrm{y}_{\mathrm{r}}} \frac{\partial \boldsymbol{\Xi}^{\mathrm{T}}}{\partial \mathrm{y}}\right] \mathbf{C}_{\mathrm{s}}^{1\ \mathrm{t}}--\mathrm{K} \boldsymbol{\Xi}^{\mathrm{T}} \mathrm{C}^{1 \mathrm{t}} \boldsymbol{\Xi}^{\mathrm{T}} \mathrm{C}^{2 \mathrm{t}}.
\end{aligned}
\tag{29}
$$

$$
\mathrm{R}\frac{\mathrm{n^f}}{\mathrm{n^s}}\frac{\boldsymbol{\Xi}^{\mathrm{T}}\mathbf{C_s^2}-\mathrm{C_r^{2t}}}{\Delta\mathrm{t}}=\frac{1}{2}\left[\mathrm{D_{xx_r}}\frac{\partial^2\boldsymbol{\Xi}^{\mathrm{T}}}{\partial\mathrm{x}^2}+\mathrm{D_{yy_r}}\frac{\partial^2\boldsymbol{\Xi}^{\mathrm{T}}}{\partial\mathrm{y}^2}\right]\mathbf{C}_{\mathrm{s}}^{2\ \mathrm{t+\Delta t}}+
\frac{1}{2}\left[\mathrm{D_{xx_r}}\frac{\partial^2\boldsymbol{\Xi}^{\mathrm{T}}}{\partial\mathrm{x}^2}+\mathrm{D_{yy_r}}\frac{\partial^2\boldsymbol{\Xi}^{\mathrm{T}}}{\partial\mathrm{y}^2}\right]\mathbf{C}_{\mathrm{s}}^{2\ \mathrm{t}}\frac{1}{2}\left[\mathrm{v_{x_r}}\frac{\partial\boldsymbol{\Xi}^{\mathrm{T}}}{\partial\mathrm{x}}+\mathrm{v_{y_r}}\frac{\partial\boldsymbol{\Xi}^{\mathrm{T}}}{\partial\mathrm{y}}\right]\mathbf{C}_{\mathrm{s}}^{2\ \mathrm{t+\Delta t}}-
\frac{1}{2}\left[\mathrm{v_{x_r}}\frac{\partial\boldsymbol{\Xi}^{\mathrm{T}}}{\partial\mathrm{x}}+\mathrm{v_{y_r}}\frac{\partial\boldsymbol{\Xi}^{\mathrm{T}}}{\partial\mathrm{y}}\right]\mathbf{C}_{\mathrm{s}}^{2\ \mathrm{t}}--\mathrm{K}\boldsymbol{\Xi}^{\mathrm{T}}\mathrm{C^{1t}}\boldsymbol{\Xi}^{\mathrm{T}}\mathrm{C^{2t}}+\mathrm{F_{release}}\left(\mathrm{t}\right)\delta\left(\mathbf{x}_{\mathrm{r}}-\mathbf{x_i}\right). \tag{30}
$$

where the seepage velocity, $\mathrm{v_x}$ and $\mathrm{v_y}$, and dispersion coefficients are determined by substituting Eq.(24) in Eq.(7) and Eq.(8) resulting in the following equations:

$$
\mathrm{v_{x_r}}=-\mathrm{k_{x_r}}\frac{\partial\boldsymbol{\Xi}^{\mathrm{T}}}{\partial\mathrm{x}}\mathbf{h}_{\mathrm{s}}\quad;\quad\mathrm{v_{y_r}}=-\mathrm{k_{x_r}}\frac{\partial\boldsymbol{\Xi}^{\mathrm{T}}}{\partial\mathrm{y}}\mathbf{h}_{\mathrm{s}}. \tag{31}
$$

$$
\begin{aligned}
\mathrm{D_{xx_r}}&=\frac{\left(-\alpha_{\mathrm{L}}\mathrm{k_{x_r}}\frac{\partial\boldsymbol{\Xi}^{\mathrm{T}}}{\partial\mathrm{x}}\mathbf{h}_{\mathrm{s}}\right)^2+\left(-\alpha_{\mathrm{T}}\mathrm{k_{y_r}}\frac{\partial\boldsymbol{\Xi}^{\mathrm{T}}}{\partial\mathrm{y}}\mathbf{h}_{\mathrm{s}}\right)^2}{\sqrt{\left(-\mathrm{k_{x_r}}\frac{\partial\boldsymbol{\Xi}^{\mathrm{T}}}{\partial\mathrm{x}}\mathbf{h}_{\mathrm{s}}\right)^2+\left(-\mathrm{k_{x_r}}\frac{\partial\boldsymbol{\Xi}^{\mathrm{T}}}{\partial\mathrm{y}}\mathbf{h}_{\mathrm{s}}\right)^2}}+\mathrm{D}^*,\\
\mathrm{D_{yy_r}}&=\frac{\left(-\alpha_{\mathrm{T}}\mathrm{k_{x_r}}\frac{\partial\boldsymbol{\Xi}^{\mathrm{T}}}{\partial\mathrm{x}}\mathbf{h}_{\mathrm{s}}\right)^2+\left(-\alpha_{\mathrm{L}}\mathrm{k_{y_r}}\frac{\partial\boldsymbol{\Xi}^{\mathrm{T}}}{\partial\mathrm{y}}\mathbf{h}_{\mathrm{s}}\right)^2}{\sqrt{\left(-\mathrm{k_{x_r}}\frac{\partial\boldsymbol{\Xi}^{\mathrm{T}}}{\partial\mathrm{x}}\mathbf{h}_{\mathrm{s}}\right)^2+\left(-\mathrm{k_{x_r}}\frac{\partial\boldsymbol{\Xi}^{\mathrm{T}}}{\partial\mathrm{y}}\mathbf{h}_{\mathrm{s}}\right)^2}}+\mathrm{D}^*.
\end{aligned} \tag{32}
$$

The accuracy and stability of the solution using the collocation method depend on imposing and implementing the boundary conditions at boundary nodes, in particular, Neumann boundary conditions. There are different methods to impose derivatives boundary conditions which have been discussed in studies (Liu and Gu, 2005). In this study, we have used the direct collocation method to implement the Neumann boundary condition. The following examples denote the implementation of the Dirichlet and Neuman boundary condition on groundwater flow equations.

$$
\begin{aligned}
&\mathrm{h}\left(\mathrm{x_1},\mathrm{y_1}\right)=\mathrm{h_0}=\boldsymbol{\Xi}^{\mathrm{T}}\mathbf{h}_{\mathrm{s}},\\
&\boldsymbol{\Xi}^{\mathrm{T}}=\{\Xi_1\ \Xi_2\ ...\ \Xi_n\}.
\end{aligned} \tag{33}
$$

$$
\begin{aligned}
&\mathrm{k_y}\frac{\partial\mathrm{h}}{\partial\mathrm{y}}|_{(\mathrm{x_n},\mathrm{y_n})}=0=\mathrm{k_{y_r}}\frac{\partial\boldsymbol{\Xi}^{\mathrm{T}}}{\partial\mathrm{y}}\mathbf{h}_{\mathrm{s}},\\
&\frac{\partial\boldsymbol{\Xi}^{\mathrm{T}}}{\partial\mathrm{y}}=\{\frac{\partial\Xi_1}{\partial\mathrm{y}}\ \frac{\partial\Xi_2}{\partial\mathrm{y}}\ ...\ \frac{\partial\Xi_{\mathrm{n}}}{\partial\mathrm{y}}\}.
\end{aligned} \tag{34}
$$

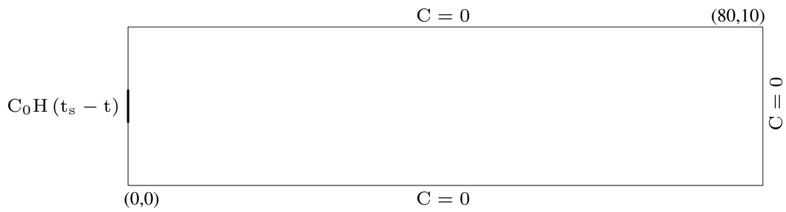

Figure 4: The aquifer domain for the analytical solution

4. Optimal shape parameter and model verification

To evaluate the performance of our simulation and find the optimum shape parameter, based on the introduced RPCM formulations, a coupled flow and reactive transport model was developed in MATLAB and the results are verified with two-dimensional contaminant transport benchmark equation. Furthermore, the results of the verified model are compared with the sandbox experiments results.

4.1. Optimal shape parameters

The following advection-diffusion transport equation with first-order decay rate constant is considered to find the optimum shape parameter

$$
\begin{gathered}
\frac{\partial \mathrm{C}}{\partial \mathrm{t}} + \frac{\rho \mathrm{b}}{\theta}\frac{\partial \mathrm{S}}{\partial \mathrm{t}} = \mathrm{D_x}\frac{\partial^2 \mathrm{C}}{\partial \mathrm{x}^2} - \mathrm{v}\frac{\partial \mathrm{C}}{\partial \mathrm{x}} + \mathrm{D_y}\frac{\partial^2 \mathrm{C}}{\partial \mathrm{y}^2} - \lambda \mathrm{C}, \\
\frac{\partial \mathrm{S}}{\partial \mathrm{t}} = \alpha \left(\mathrm{K_d C} - \mathrm{S}\right).
\end{gathered}
\tag{35}
$$

where C is the contaminant concentration $\left[\mathrm{ML}^3\right]$, ρ_b is the Bulk density of soil $\left[\mathrm{ML}^3\right]$, θ is soil porosity, S is Sorbed concentration $\left[\mathrm{MM}^{-1}\right]$, $\mathrm{D_x}$ and $\mathrm{D_y}$ are diffusion coefficients in x and y directions $\left[\mathrm{L}^2\mathrm{T}^{-1}\right]$, λ is first-order decay rate constant $\left[\mathrm{T}^{-1}\right]$, α is first-order decay rate constant $\left[\mathrm{T}^{-1}\right]$ and $\mathrm{K_d}$ is sorption distribution coefficient.
The initial and boundary conditions are (Fig. 4) ,

$$
\begin{aligned}
&\mathrm{C}\left(\mathrm{x},\mathrm{y},0\right) = 0 \quad ; \quad \mathrm{S}\left(\mathrm{x},\mathrm{y},0\right) = 0, \quad (\mathrm{x},\mathrm{y}) \in \Omega, \\
&\mathrm{C}\left(0,\mathrm{y},\mathrm{t}\right) = \begin{cases} \mathrm{C_0 H}\left(\mathrm{t_s} - \mathrm{t}\right) & \mathrm{y_b} \leqslant \mathrm{y} \leqslant \mathrm{y_t} \\ 0 & \end{cases}, \\
&\frac{\partial \mathrm{C}}{\partial \mathrm{x}} = 0 \;\; ; \;\; \frac{\partial \mathrm{C}}{\partial \mathrm{y}} = 0 \qquad\qquad (\mathrm{x},\mathrm{y}) \in \Gamma_N.
\end{aligned}
\tag{36}
$$

The analytical solution to this problem in laplace domain been given by (Goltz and Huang, 2017)

$$
\overline{\mathrm{C}}\left(\mathrm{x},\mathrm{y},\mathrm{s}\right) = \frac{1 - \exp\left(-\mathrm{t_s s}\right)}{\mathrm{b}}\left[\hat{\overline{\mathrm{C}}}\left(0\right) + 2\sum_{i=1}^{\mathrm{N}}\hat{\overline{\mathrm{C}}}\left(n\right)\sin\left(\frac{\mathrm{n}\pi\mathrm{y}}{\mathrm{b}}\right)\right].
\tag{37}
$$

$$
\begin{aligned}
&\hat{\bar{\mathrm{C}}}(\mathrm{n}) = \gamma \exp(\mathrm{rx}),\\
&\gamma = \frac{\mathrm{C_0 b}}{\mathrm{s n}\pi}\left[\sin\left(\frac{\mathrm{n}\pi \mathrm{y_t}}{\mathrm{b}}\right) - \sin\left(\frac{\mathrm{n}\pi \mathrm{y_b}}{\mathrm{b}}\right)\right],\\
&\mathrm{r} = \frac{1}{2\mathrm{D_x}}\left(\mathrm{v} - \sqrt{\mathrm{v}^2 + 4\mathrm{D_x}\boldsymbol{\beta}}\right),\\
&\boldsymbol{\beta} = \mathrm{D_y}\left(\frac{\mathrm{n}\pi}{\mathrm{b}}\right)^2 + \Theta,\\
&\Theta = (\mathrm{s} + \lambda) + \frac{\rho_b \alpha \mathrm{k_d s}}{\theta\,[s + \alpha]}.
\end{aligned}
\tag{38}
$$

where x and y are the coordinates in x and y directions respectively, s is Laplace complex variable, $\mathrm{C_0}$ is the concentration at contaminant source, b is the aquifer width. The physical constants and parameters for the corresponding analytical solution are summarized in table 2. To find the optimum value for α_c and q in the Eq.(15), the

Parameters	Value
Porosity, θ	0.25
Bulk density of soil, ρ_b	1.5 kg/L
Diffusion coefficient in x direction,$\mathrm{D_x}$	0.2 $\mathrm{m^2/min}$
Diffusion coefficient in y direction$\mathrm{D_y}$	0.02 $\mathrm{m^2/min}$
Seepage velocity v	1 $\mathrm{m/min^{-1}}$
Contaminant concentration at source	3500 $\mathrm{mg/L}$
Sorption distribution coefficient $\mathrm{k_d}$	1
First-order decay rate constant λ	0.001 $\mathrm{m^2/min}$
First-order desorption rate constant α	1 $\mathrm{min^{-1}}$

Table 1: the parameters values for analytical solution

sensitive analysis was done. In the analysis, first, the parameter q was varied from 0.8 to 1.2 for different α_c and a relative error of concentration was defined as follows:

$$
\mathrm{RE} = \frac{\sum_{\mathrm{i=0}}^{\mathrm{n}} \mid \mathrm{C_i^{exact}} - \mathrm{C_i^{RPCM}} \mid}{\sum_{\mathrm{i=0}}^{\mathrm{n}} \mid \mathrm{C_i^{exact}} \mid}. \tag{39}
$$

where $\mathrm{C_i^{exact}}$ and $\mathrm{C_i^{RPCM}}$ are contaminant concentration computed by the MQ-RBF and analytical solution, respectively. Fig. 5 Fig. 4 demonstrates the variation of relative errors of concentration with shape parameters. It can be seen, the optimal shape parameter q occurred around 1, and the minimum error is for q=0.97. Fig. 5a shows the effect of the shape parameter α_c on the contaminant concentration profile at point (30,7) for q=0.97 and compares with the exact solution. It is found that for the MQ-RBF, the values of the shape the range of 3-5 gave very good accuracy. Among different shape parameters α_c , $\alpha_\mathrm{c} = 4$ is the optimum value. Fig. 5 b compares contaminant concentration profile for the point located at (30,7) for different shape parameters q for $\alpha_\mathrm{c} = 4$. Fig. 6 compares contaminant concentration contours the MQ-RBF and analytical solutions for two-dimensional transport from a continuous line source in a confined aquifer.

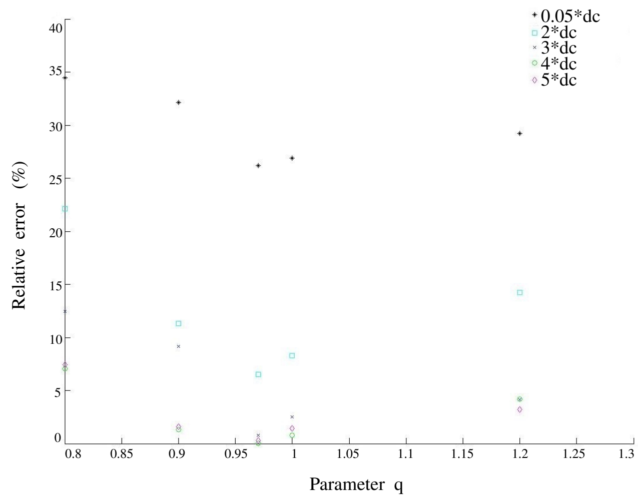

Figure 5: The relative error of concentration for different shape parameter q

The simulation has done for t = 200 min. Fig. 6 compares contaminant concentration contours of the MQ-RBF and analytical solutions for two-dimensional transport from a continuous line source. The simulation has done for t = 200 min, and the results are in good agreement.

4.2. Model verification with the sandbox experiment

A point source of 0.5% w/v potassium permanganate solution was constructed in a sandbox to map the change groundwater plume distribution over time. The sandbox is 150 cm in length, 38 cm in height, and has a thickness of 10 cm and was constructed with Plexiglass. The sandbox is 150 cm in length, 38 cm in height, and has a thickness of 10 cm and was constructed with Plexiglass. The sandbox has no-flow boundaries on top and bottom and the ends of the tanks consist of constant head tanks which are separated from the rest of the box by one impermeable wall and one perforated steel mesh filter to separate the sand from the head tanks. A peristaltic pump (Watson Marlow), which is capable of delivering a maximum of $42\ \mathrm{L/h}$, was used to circulate water through the system. The characteristics of the used sand including hydraulic conductivity were measured and given in Table 1 (Nijp et al., 2017; Sarki et al., 2014). To mitigate the creation of preferential pathways and air bubbles, the tank was filled with a layer of a few centimeters dry sand, after which tap water was added to saturate and cover the sand. More dry sand was layered over this now saturated sand, and itself covered with tap water. This process was repeated until the tank was full. The injection rate

	Size	Hydraulic conductivity	Porosity
Sand	5.00-2.36 mm	2.754 10-4 m/sec	43.3

Table 2: The characteristics of sand

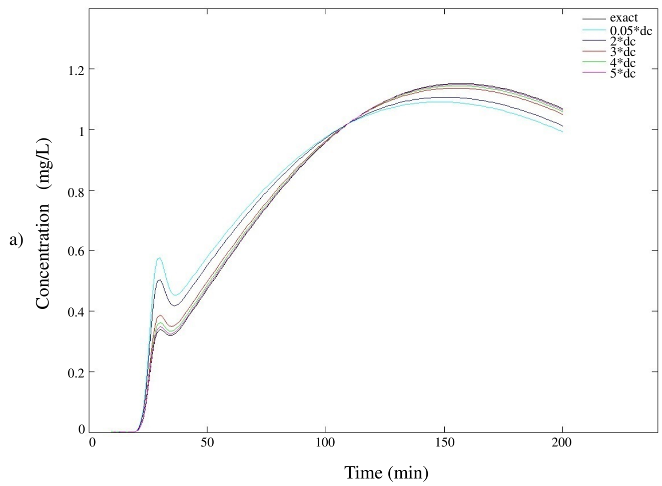

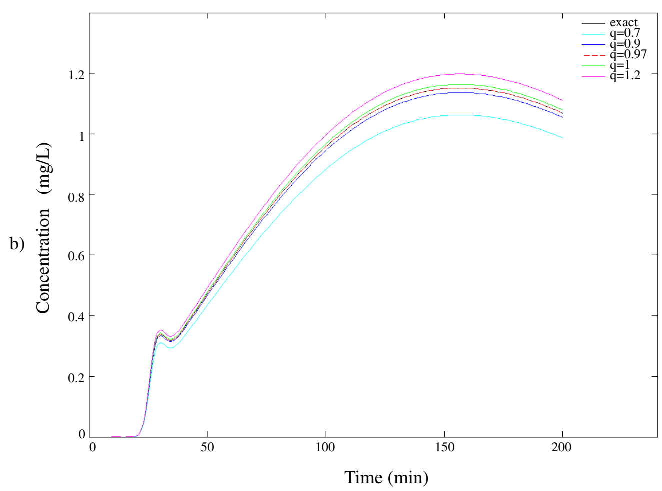

Figure 6: Shape parameter effect on the contaminant concentration profile at point (30,7) a) shape parameter α_c b) shape parameter q.

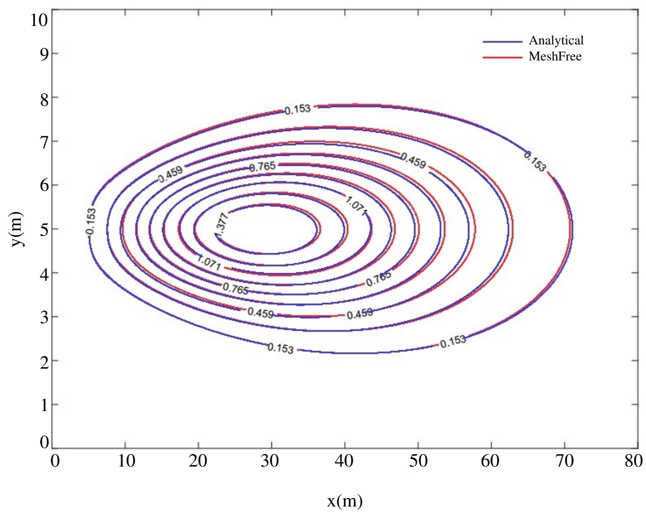

Figure 7: Comparison of the MFree and Analytical solutions for two-dimensional transport

was $16\ \mathrm{L/h}$; and 9 L total volume injected. The experiment was repeated three times, and presented results are the average results. Fig. 8 compares the observed permanganate plume in the tank and predicted plume at the same time after injection. Table 3 compares measured permanganate concentration at two different sampling points located at (36,18.5) cm and (56,18.5) cm, with respect to the origin which is located at the bottom Corner of input end of tank, with Meshfree predicted concentration.

5. Remediation design optimization using Genetic Algorithm

Multi-objective optimisation (MOO) including multi-objective genetic algorithm can be utilised to address optimization problems related to groundwater. In this study, the multi-objective genetic algorithm is employed to seek the global optimisation of remediation design. The cost of remediation and the concentration of the contaminant are competitive functions which are considered as two objective functions. To find optimal design, GA simultaneously minimises the cost of the remediation process by the minimising the number of oxidant sources and contaminant concentration by maximising the region where contaminant concentration is equal-less than the desired final concentration. To achieve this goal, we have defined the following functions:

$$\begin{aligned} &\mathrm{GA1} = \mathrm{TC} = \mathrm{n_{OS}} * \mathrm{COS}, \\ &\mathrm{GA2} = \Omega_{\mathrm{C^1_{ARCC}}} = \{(\mathrm{x},\mathrm{y}) \in \Omega : \mathrm{C^1} \leqslant \mathrm{C^1_{ARCC}}\}. \end{aligned} \tag{40}$$

where $\mathrm{C^1_{ARCC}}$ is the aimed remediation contaminant concentration, TC is the total cost of the remediation process, $\mathrm{n_{OS}}$ is the number of the oxidant sources and COS

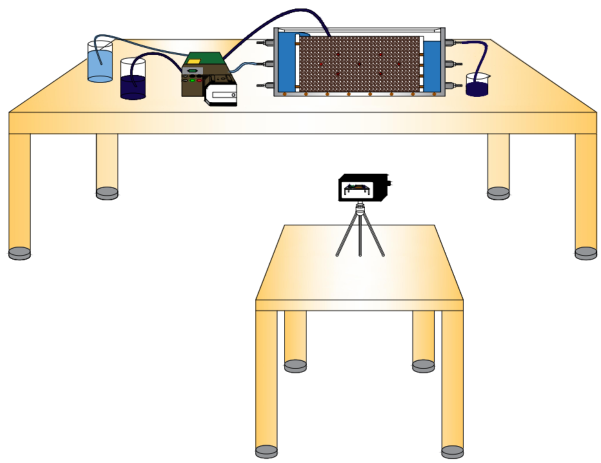

Figure 8: Schematic representation of sandbox experimental setup

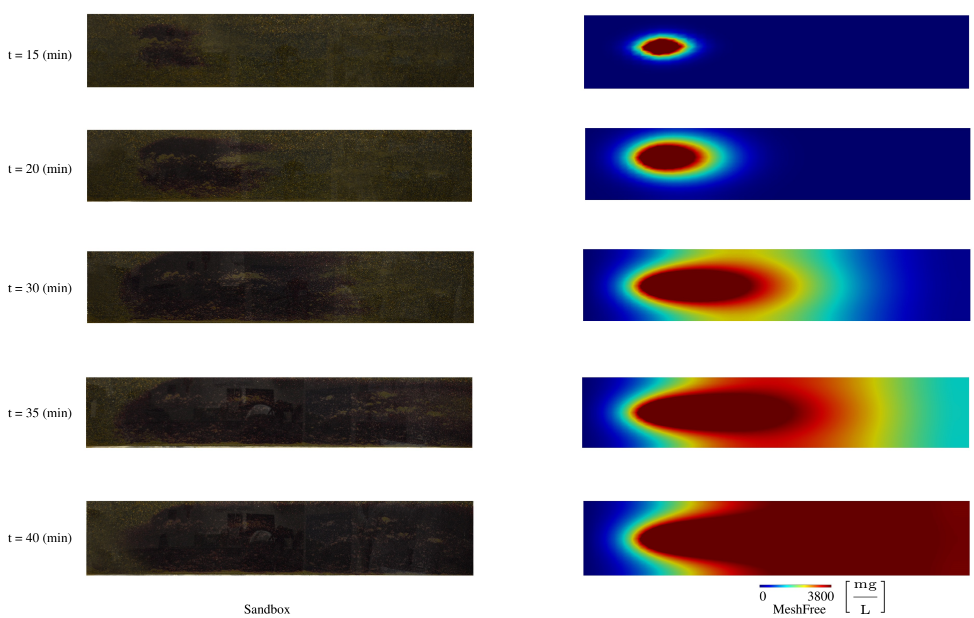

Figure 9: The comparison between observed and MFree predicted plume

Time (min)	sample point number	measured concentration (mg/L)	MFree predicted concentration (mg/L)	RMSE
5	1	3050	3040	0.32
	2	2060	2050	0.48
10	1	3080	3070	0.32
	2	2540	2530	0.39
15	1	3200	3190	0.31
	2	2850	2839	0.38
20	1	3630	3619	0.30
	2	3300	3289	0.33
25	1	3730	3719	0.29
	2	3630	3618	0.33
30	1	3720	3709	0.29
	2	3690	3679	0.29
35	1	3760	3749	0.29
	2	3710	3699	0.29
40	1	3790	3779	0.29
	2	3750	3729	0.29

Table 3: Comparison of permanganate measured concentration at sampling points to Meshfree predicted concentration.

denotes the cost of each oxidant source. To achieve the objective of the study, we wish to minimise GA1 and maximise GA2.

$$\begin{aligned} &\min \mathrm{GA1}, \\ &\max \mathrm{GA2}. \end{aligned} \tag{41}$$

by considering the following constraints:

1. the distance between oxidant sources

$$\mathrm{d} \geq \mathrm{d_c}. \tag{42}$$

where $\mathrm{d} = \sqrt{(\mathrm{x_i} - \mathrm{x_j})^2 + (\mathrm{y_i} - \mathrm{y_j})^2}$ is actual distance between oxidant source i and j and $\mathrm{d_c}$ is the critical distance between oxidant sources. The critical distance is the distance between two oxidant sources which their influence domain overlap more than %75. The influence domain is defined as a region in where the oxidant concentration reaches 15% of its initial concentration at the source after 50 days if it implements alone. The following function defines the influence domain which is used to define critical distance.

$$\Omega_{\mathrm{C^2_{20\%}}}^{\mathrm{t\,=\,50\ days}} = \{(\mathrm{x},\mathrm{y}) \in \Omega : \mathrm{C}^2 \geqslant 15\%\ \mathrm{C}_0^2\}. \tag{43}$$

regarding our prior simulation, if a distance between sources is less than the critical distance then the contaminant concentration in the whole geometry is in many designs more than aimed remediation contaminant concentration.

2. the number of oxidant sources

$$\mathrm{n_{OS}} \leq 5. \tag{44}$$

where $\mathrm{n_{OS}}$ is actual the number of oxidant sources.

6. Results and Discussions

The purpose of our numerical study is to find the optimum remediation design utilising permanganate. The aquifer domain is 500 m by 100 m with a relatively homogenous hydraulic conductivity. The oxidant sources have been considered to remediate the continuous line contaminant source and GA approach is used to find the optimum location and number of them concerning criteria presented in Section 5. The optimum shape parameter $\mathrm{q} = 0.97$ and 4.dc with 12 nodes in every support domain were used in numerical approach. The same nodes distribution used for both flow model and the transport model. The longitudinal dispersivity α_L for this problem is considered 15 m and the transverse dispersivity α_T is taken as 10% of the longitudinal dispersivity. The functions presented by (Wolf, 2013; Yao et al., 2016) are modified for our study to simulate the oxidant release. The contaminant concentration at line source located at $\mathrm{x} = 60\ \mathrm{m}, 20\ \mathrm{m} \leq \mathrm{y} \leq 80\ \mathrm{m}$ is $\mathrm{C}^1 = 275\frac{\mathrm{mg}}{\mathrm{L}}$. Fig. 9a demonstrates the piezometric head iso head contours. Fig. 9b and 9c show the contaminant and oxidant concentration at different times. The simulations have been performed for 250 days with a time step of 0.004 day. Overall, the water head contours decreased from left to right, with mounding around the contaminant and the oxidant injection sources. As expected, the concentration of the contaminant in the regions closer to the oxidant sources is less than the farther regions, but with the increase the distances from the oxidant sources it changes rapidly. The performance of the optimized design was compared with two different arbitrary design. In both designs, three oxidant sources were considered locating at (90, 30) m, (90, 70) and (150, 50) in the first design and (110, 50) m, (110, 30) and (250, 70) in the second design. Fig. 10 compares the contaminant concentration at three different observation points located at the (100,50) m, (150,65) m and (300,55) m at the downside of the stream for optimised design and arbitrary designs. The optimisation of remediation not only decrease the contaminant concentration at observation points but also it postpone the time in when the concentration begins to increase from zero in the observation points expects the second arbitrary design at the third observation point. The delay time was almost 12, 37 and 34 days in the first arbitrary design and 17, 48 and -4 days in the second arbitrary design for first, second and third observation points respectively. Furthermore, it can be translated that optimisation design reduces the remediation cost. Because to reach the same level of the contaminant concentration in the arbitrary designs, either the initial oxidant concentration at sources must be 8% and 11%, in the first and second arbitrary design respectively, higher than the optimized design or with the same initial oxidant concentration higher number of oxidant sources is needed, for example, to reach almost same contaminant concentration four oxidant sources which are located at (90,30),(90,70),(100,40) and (100,60) is

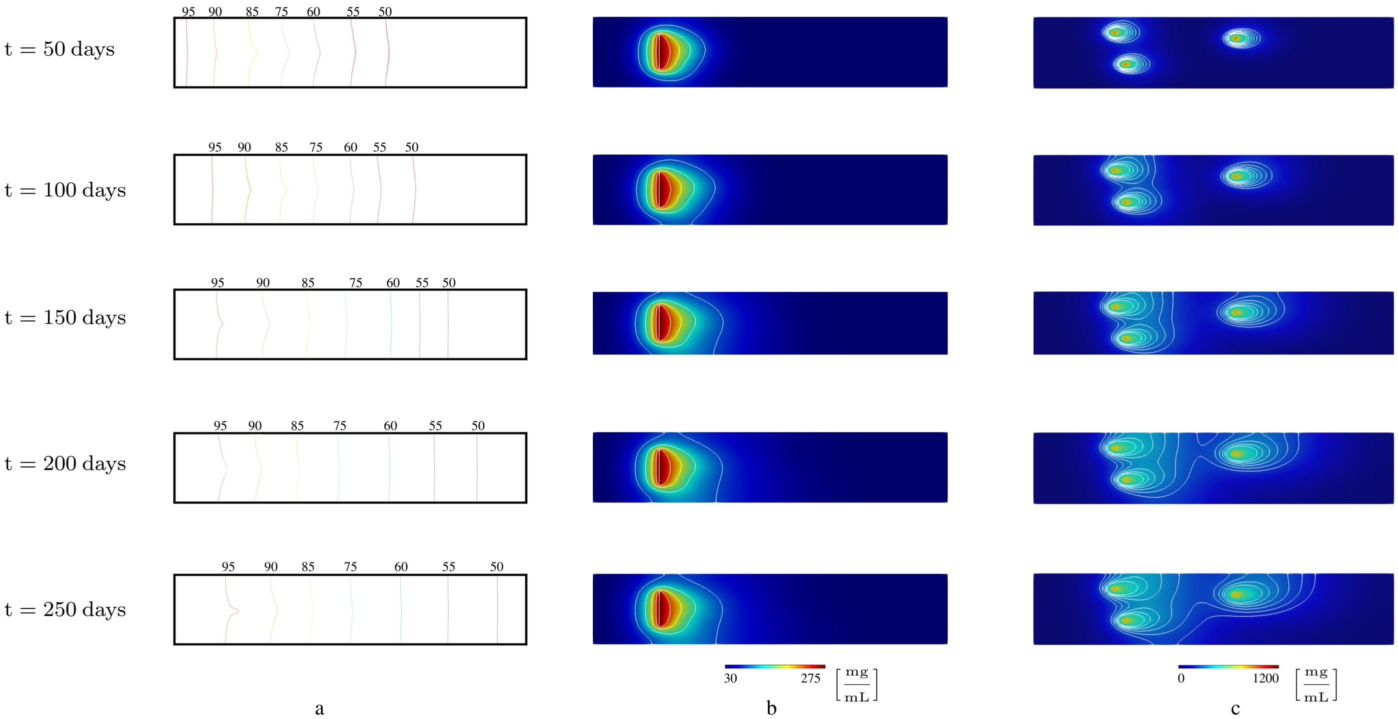

Figure 10: a:piezometric head profile and contours, b: contaminant concentration profile, c: oxidant concentration profile.

necessary. In addition, it can be concluded that the far further from the centre line of the geometry the higher delay. In all observation points, the effect of optimization on the contaminant concentration is decreased with increasing the time. The contaminant concentration after 250 days was 17.1 %, 21.8 % and 22.4 % in the first arbitrary design 48.8 %, 57.8 % and -28.7 % in the second arbitrary design for first, second and third observation points respectively, less than it values in the optimised design.

7. Conclusion

In this study, a multi quadratic radial basis function was used to simulate coupled groundwater flow and reactive transport of contaminant and oxidant in a porous aquifer. The sensitive analysis was done to find the optimum used shape parameter in MQ-RBFs with comparing the results with two-dimensional solute transport benchmark. The output from the model is compared to the results of sandbox experiment.

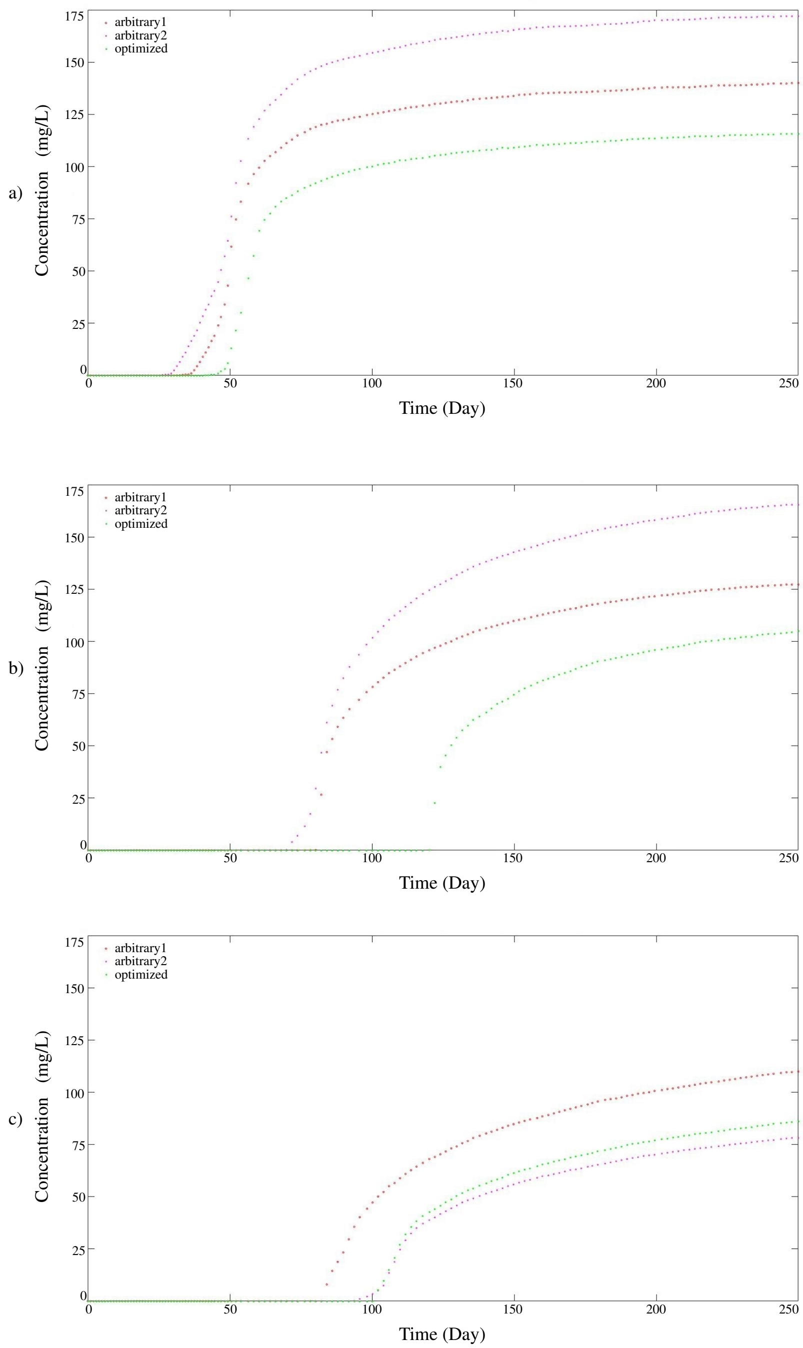

Figure 11: the contaminant concentration profile at observation point located at a) (100,50) m, b) (150,65) m, c) (300,55) m.

The RSME error between measured and predicted permanganate concentration at two sample points for different times was less than 0.5, and it shows that the measured and predicted concentration are in good agreement. It was observed that the predicted permanganate concentration by the meshfree method shows good agreement with the measured values of the permanganate concentration in physical sandbox model. The genetic algorithm was used to find the optimum number and the optimum design of the oxidant sources regarding introduced criteria in section 5. The optimization has two different effects on the remediation process. It not only delays the reaching time of the contaminant to the downstream region but also it decreases the contaminant concentration in this area.

Acknowledgement

This work was completed as part of the REMEDIATE (Improved decision-making in contami- nated land site investigation and risk assessment) Marie-Curie Innovation Training Network. The network has received funding from the European Unions Horizon 2020 Programme for research, technological development and demonstration under grant agreement n. 643087. REMEDIATE is coordinated by the QUESTOR Centre at Queens University Belfast http://questor.qub.ac.uk/REMEDIATE/

References

An, D., Yang, Y., Jiang, Y., Xi, B., Bai, S., Li, M., Zhang, J., 2013. A new risk ranking method for groundwater contamination of hazardous waste landfills in China. Vol. 22.

Ba, D. A., Mayer, A. S., 2007. Data-worth analysis for multiobjective optimal design of pump-and-treat remediation systems. Advances in Water Resources 30 (8), 1815–1830.

Bear, J., 1979. Hydraulics of groundwater. McGraw-Hill International Book Co.

Bear, J., 2007. Hydraulics of Groundwater. Dover Publications.

Bertolazzi, E., Manzini, G., 2004. A finite volume method for transport of contaminants in porous media. Applied Numerical Mathematics 49 (3), 291–305.

Chen, Y., Lu, H., Li, J., Ren, L., He, L., 2017. A leader-follower-interactive method for regional water resources management with considering multiple water demands and eco-environmental constraints. Journal of Hydrology 548 (Supplement C), 121–134.

Elimelech, M., Phillip, W. A., 2011. The future of seawater desalination: Energy, technology, and the environment. Science 333 (6043), 712–717.

Freeze, R., Cherry, J., 1979. Groundwater. Prentice-Hall.

Goltz, M., Huang, J., 2017. Modeling. John Wiley & Sons, Inc., pp. 1–17.

GR, L., 1999. A point assembly method for stress analysis for solid, in impact response of materials & structures. V. P. W. Shim et al. eds, 475–480.

Guneshwor Singh, L., Eldho, T. I., Vinod Kumar, A., 2016. Coupled groundwater flow and contaminant transport simulation in a confined aquifer using meshfree radial point collocation method (rpcm). Engineering Analysis with Boundary Elements 66 (Supplement C), 20–33.

Hadley, P. W., Newell, C. J., 2012. Groundwater remediation: The next 30 years. Ground Water 50 (5), 669–678.

Hardy, R. L., 1971. Multiquadric equations of topography and other irregular surfaces. Journal of Geophysical Research 76 (8), 1905–&.

He, L., Huang, G. H., Lu, H. W., 2008a. A simulation-based fuzzy chance-constrained programming model for optimal groundwater remediation under uncertainty. Advances in Water Resources 31 (12), 1622–1635.

He, L., Huang, G. H., Lu, H. W., 2009. A coupled simulation-optimization approach for groundwater remediation design under uncertainty: An application to a petroleum-contaminated site. Environmental Pollution 157 (8), 2485–2492.

He, L., Huang, G.-h., Lu, H.-w., Zeng, G.-m., 2008b. Optimization of surfactant-enhanced aquifer remediation for a laboratory btex system under parameter uncertainty. Environmental Science & Technology 42 (6), 2009–2014.

Holland, J. H., 1992. Adaptation in Natural and Artificial Systems: An Introductory Analysis with Applications to Biology, Control and Artificial Intelligence. MIT Press.

Huang, G., 1992. A stepwise cluster analysis method for predicting air quality in an urban environment. Atmospheric Environment. Part B. Urban Atmosphere 26 (3), 349–357.

Illman, W. A., Berg, S. J., Yeh, T.-C. J., 2012. Comparison of approaches for predicting solute transport: Sandbox experiments. Ground Water 50 (3), 421–431.

JG Wang, G. L., 2002. A point interpolation meshless method based on radial basis functions. International Journal for Numerical Methods in Engineering 54 (11), 1623–1648.

Kansa, E. J., 1990. Multiquadricsa scattered data approximation scheme with applications to computational fluid-dynamicsii solutions to parabolic, hyperbolic and elliptic partial differential equations. Computers & Mathematics with Applications 19 (8), 147–161.

Leo, C. J., Booker, J. R., 1998. A boundary element method for analysis of contaminant transport in fractured and non-fractured porous media. Computers and Geotechnics 23 (3), 165–181.

Liu, G., Gu, Y., 2005. An Introduction to Meshfree Methods and Their Programming. Springer Netherlands.

Meenal, M., Eldho, T. I., 2011. Simulation of groundwater flow in unconfined aquifer using meshfree point collocation method. Engineering Analysis with Boundary Elements 35 (4), 700–707.

Meenal, M., Eldho, T. I., 2012. Two-dimensional contaminant transport modeling using meshfree point collocation method (pcm). Engineering Analysis with Boundary Elements 36 (4), 551–561.

Nijp, J. J., Metselaar, K., Limpens, J., Gooren, H. P. A., van der Zee, S. E. A. T. M., 2017. A modification of the constant-head permeameter to measure saturated hydraulic conductivity of highly permeable media. MethodsX 4, 134–142.

Praveen Kumar, R., Dodagoudar, G. R., 2008. Two-dimensional modelling of contaminant transport through saturated porous media using the radial point interpolation method (rpim). Hydrogeology Journal 16 (8), 1497.

Ricken, T., Sindern, A., Bluhm, J., Widmann, R., Denecke, M., Gehrke, T., Schmidt, T., 2014. Concentration driven phase transitions in multiphase porous media with application to methane oxidation in landfill cover layers. ZAMM - Journal of Applied Mathematics and Mechanics / Zeitschrift fr Angewandte Mathematik und Mechanik 94 (78), 609–622.

Rippa, S., 1999. An algorithm for selecting a good value for the parameter c in radial basis function interpolation. Advances in Computational Mathematics 11 (2-3), 193–210.

Robeck, M., Ricken, T., Widmann, R., 2011. A finite element simulation of biological conversion processes in landfills. Waste Management 31 (4), 663–669.

Sarki, A., Mirjat, M. S., Mahessar, A. A., Kori, S. M., Qureshi, A. L., 2014. Determination of saturated hydraulic conductivity of different soil texture materials. IOSR J ournal of Agriculture and Veterinary Science 7 (12), 56–62.

Schaback, R., Wendland, H., 2000. Adaptive greedy techniques for approximate solution of large rbf systems. Numerical Algorithms 24 (3), 239–254.

SCHMUCK, S., WERNER, D., WIDMANN, R., RICKEN, T., 2016. Depsim: Numerical 3d-simulation of the water, gas and solid phase in a landfill. International Journal of Sustainable Development and Planning 11 (5), 694 – 699.

Seyedpour, S. M., Ricken, T., 2016. Modeling of contaminant migration in groundwater: A continuum mechanical approach using in the theory of porous media. PAMM 16 (1), 487–488.

Sharma, H. D., Reddy, K. R., 2004. Geoenvironmental engineering: site remediation, waste containment, and emerging waste management technologies. John Wiley & Sons, Inc.

Sinha, E., Minsker, B. S., 2007. Multiscale island injection genetic algorithms for groundwater remediation. Advances in Water Resources 30 (9), 1933–1942.

Sotomayor, G., Hampel, H., Vzquez, R. F., 2018. Water quality assessment with emphasis in parameter optimisation using pattern recognition methods and genetic algorithm. Water research 130, 353–362.

Stroo, H. F., Leeson, A., Ward, C. H., 2012. Bioaugmentation for groundwater remediation. Vol. 5. Springer Science & Business Media.

Sun, N.-Z., Sun, A., 2013. Mathematical modeling of groundwater pollution. Springer Science & Business Media.

Tam, E. K. L., Byer, P. H., 2002. Remediation of contaminated lands: a decision methodology for site owners. Journal of Environmental Management 64 (4), 387–400.

Tatalovich, M. E., Lee, K. Y., Chrysikopoulos, C. V., 2000. Modeling the transport of contaminants originating from the dissolution of dnapl pools in aquifers in the presence of dissolved humic substances. Transport in Porous Media 38 (1), 93–115.

Tian, N., Sun, J., Xu, W., Lai, C.-H., 2011. An improved quantum-behaved particle swarm optimization with perturbation operator and its application in estimating groundwater contaminant source. Inverse Problems in Science and Engineering 19 (2), 181–202.

Varghese, G. K., Alappat, B. J., Samad, M. S. A., 2015. Mt3dms and genetic algorithm in environmental forensic investigations. Procedia Environmental Sciences 30, 85–90.

Wang, H., Anderson, M. P., 1982. Introduction to groundwater modeling : finite difference and finite element methods. W.H. Freeman, San Francisco.

Wang, J. G., Liu, G. R., 2002. On the optimal shape parameters of radial basis functions used for 2-d meshless methods. Computer Methods in Applied Mechanics and Engineering 191 (23-24), 2611–2630.

Wolf, G., 2013. Slow release permanganate cylinders for sustainable in situ chemical oxidation: Development of a conceptual design tool (m.s. thesis),. Clarkson University, Potsdam, NY.

Wright, G., 2003. Radial Basis Function Interpolation: Numerical and Analytical Developments. University of Colorado.

Yao, G., Bliss, K. M., Crimi, M., Fowler, K. R., Clark-Stone, J., Li, W., Evans, P. J., 2016. Radial basis function simulation of slow-release permanganate for groundwater remediation via oxidation. Journal of Computational and Applied Mathematics 307 (Supplement C), 235–247.

Zhang, S., Mao, G., Crittenden, J., Liu, X., Du, H., 2017. Groundwater remediation from the past to the future: A bibliometric analysis. Water Research 119 (Supplement C), 114–125.

Zheng, C., Bennett, G. D., 2002. Applied contaminant transport modeling. Vol. 2. Wiley-Interscience New York.